Research Article | Vol. 29, No. 22 / 25 Oct 2021 / Optics Express 35414
Optics EXPRESS

Tomographic refractive index profiling of direct laser written waveguides

NICOLAS BARRÉ,[1,*] RAVI SHIVARAMAN,[2] LISA ACKERMANN,[3,4] SIMON MOSER,[1] MICHAEL SCHMIDT,[3,4] PATRICK SALTER,[2] MARTIN BOOTH,[2,4] AND ALEXANDER JESACHER[1,4]

[1]*Institute of Biomedical Physics, Medical University of Innsbruck, Müllerstraße 44, 6020 Innsbruck, Austria*
[2]*Department of Engineering Science, University of Oxford, Parks Road, Oxford OX1 3PJ, UK*
[3]*Institute of Photonic Technologies, Friedrich-Alexander-University Erlangen-Nürnberg, Konrad-Zuse-Straße 3/5, Erlangen 91052, Germany*
[4]*Erlangen Graduate School in Advanced Optical Technologies (SAOT), Friedrich-Alexander-University Erlangen-Nürnberg, Paul-Gordan-Straße 6, 91052 Erlangen, Germany*
[*]*nicolas.barre@i-med.ac.at*

Abstract: The fabrication of complex integrated photonic devices via direct laser writing is a powerful and rapidly developing technology. However, the approach is still facing several challenges. One of them is the reliable quantitative characterization of refractive index (RI) changes induced upon laser exposure. To this end, we develop a tomographic reconstruction algorithm following a modern optimization approach, relying on accelerated proximal gradient descent, based on intensity images only. Very recently, such algorithms have become the state of the art in the community of bioimaging, but have never been applied to direct laser written structures such as waveguides. We adapt the algorithm to our concern of characterizing these translation-invariant structures and extend it in order to jointly estimate the aberrations introduced by the imaging system. We show that a correct estimation of these aberrations is necessary to make use of data recorded at larger angles and that it can increase the fidelity of the reconstructed RI profiles. Moreover, we present a method allowing to cross-validate the RI reconstructions by comparing en-face widefield images of thin waveguide sections with matching simulations based on the retrieved RI profile.

1. Introduction

The direct manufacture of photonic structures inside transparent dielectrics using ultra short pulsed lasers is rapidly developing. Focusing light of sufficient energy alters materials at the nanoscale via the formation of a free electron plasma, causing permanent local modifications of the atomic structure. The quality of these modifications can vary strongly. Depending on laser parameters and material properties, the net effect can be a decreased or increased refractive index (RI) [1], the formation of birefringent nanogratings [2] or voids [3,4], an increased solubility in chemical agents which can be used to etch microchannels [5,6], or even a change of electric conductivity [7–9]. This wide range of possible modifications has enabled the fabrication of an entirely novel family of fully integrated photonic devices, ranging from passive tools such as directional couplers and wavelength demultiplexers, to active waveguide amplifiers and lasers [1].

Embedded waveguides often represent the "building blocks" of these photonic devices and the quality of their fabrication is thus of particular importance. At the same time the high complexity of the laser-matter interaction in conjunction with small, undesired variations in the optical setup or laser beam profile make it difficult to reliably predict the manufactured RI profile solely from laser parameters such as pulse energy and repetition rate. This makes it often necessary to inspect

#434846 https://doi.org/10.1364/OE.434846
Journal © 2021 Received 22 Jun 2021; revised 10 Sep 2021; accepted 17 Sep 2021; published 14 Oct 2021

Optics EXPRESS

the waveguides after fabrication. Several techniques have been applied to this end. The Refracted Near-field [10–12], and micro-reflectivity [13] methods have been shown to be precise, but demand direct access to the waveguide's polished end facet and therefore require some preceding treatment steps of the substrate. Furthermore, these techniques only provide information about a single cross section and don't permit an overall assessment along the entire guiding structure.

Ideally, quality monitoring would be happening in situ, that is directly in the fabrication setup, in order to facilitate a fine tuning of the manufacturing parameters until the desired profile is obtained. In the most commonly used writing geometry, where the substrate is laterally translated underneath the objective lens, this would imply that only information from viewing angles that are mostly about orthogonal to the waveguide axis can be collected. In this geometry, it is relatively straightforward to infer the accumulated phase change across a waveguide using quantitative phase imaging techniques [14], but much harder to estimate the actual 2D RI profile, which ultimately determines the guiding properties.

Diffraction tomography represents a potential solution to this problem. However, although it has been applied to traditional glass-pulled waveguides [15,16], it remains unclear if and to which extent these methods are able to reveal structural details of direct laser written guides, which can be far less rotationally symmetric and exhibit small relative RI changes on the order of 10^{-3}. Existing studies on this topic have either amplified the signal by diffraction off many identical waveguides [17] or used basic tomographic implementations that did not aim at retrieving a quantitative RI profile [18]. In the present work we investigate the feasibility of diffraction tomography for the measurement of waveguide RI profiles manufactured by femtosecond (fs) laser irradiation in glass.

For quality assessment, thin waveguide slices are cut off the glass substrate and "en face" widefield imaged. Such widefield images are susceptible to even small RI profile changes, which we prove by numerical simulations. The experimental slice images are compared to matching simulations derived from the tomographic RI profiles. We find that the tomography results allow for precise predictions of the observed slice images, thus indicating a precise recovery of the RI profile.

Finally, we show that phase aberrations, which often exist in high aperture optical systems, can significantly degrade the information contained in images taken under high tomographic angles. We present an algorithmic approach to estimate aberrations jointly with the waveguide profile and demonstrate its feasibility.

2. Methods

2.1. Manufacturing of waveguides

All the waveguides employed in the study were fabricated inside Corning Eagle 2000 glass substrates. The writing was performed using a femtosecond laser (Pharos SP - Light Conversion Systems) operating at a wavelength of 514 nm, a pulse repetition rate of 1 MHz and a pulse duration of 170 fs. A 0.5 NA/20× Zeiss EC Plan-NEOFLUAR microscope objective was used to focus the fabrication laser at a depth of 150 µm beneath the substrate surface. The sample was then translated at a speed of 2 mm/s transverse to the laser write beam, as sketched in Fig. 1(a), with the laser power varied in the range 30 mW to 80 mW. The fabrication system incorporated a liquid crystal spatial light modulator (SLM) to control the phase of the laser at the pupil plane of the fabrication objective lens, as described in [19].

2.2. Tomographic imaging

The tomography setup, sketched in Fig. 1(b), uses a 1.4 NA oil immersion lens (Olympus UPlanSApo, 100x) and a 1.4 NA oil condenser (Olympus U-AAC). Light of a blue LED (Thorlabs M455D3) is focused onto a 100 µm sized pinhole and collimated with a 200 mm lens to obtain

Optics EXPRESS

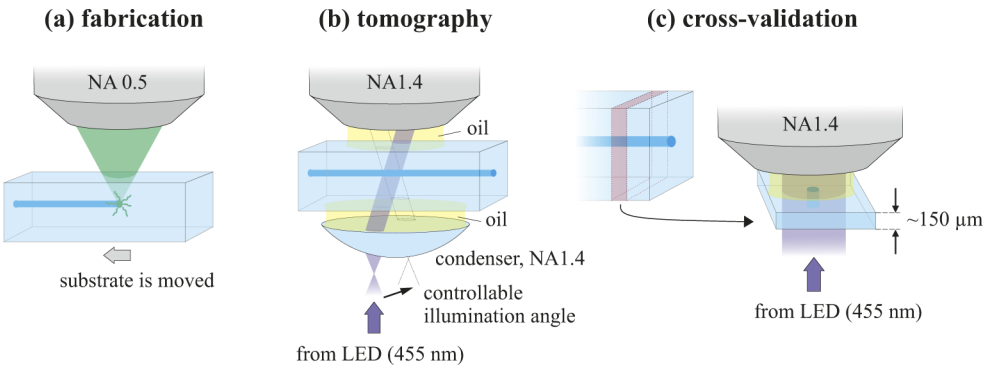

Fig. 1. Graphical illustrations of our experimental procedures (a) waveguide writing, (b) tomographic imaging and (c) cross-validation by taking en-face images of waveguide cross-sections.

high spatial coherence. The beam is reflected off a mirror in a mechanical tip/tilt mount with home-built motorization. Using 4f relay optics, the pinhole is imaged into the back focal plane of the condenser with a magnification of 3/4. The motorized mirror allows us to steer the pinhole image to arbitrary positions within the condenser pupil and thus to establish any illumination NA up to 1.35 (63 deg. in the sample substrate). The images are formed by a microscope tube lens (Nikon, f = 200 mm, Edmund Optics #58-520) on the sensor of a CCD camera (Basler pulse puA1600-60uc). A piezoelectric holder (Piezosystem Jena MIPOS 100) allows fine tuning the objective position in a range of 100 µm.

A typical tomographic image set consist of 42 images of a waveguide, taken at illumination angles ranging between ± 45 deg. around the axis defined by the waveguide. A second image set is taken at identical angles, but with the waveguide sample translated such that only the background is recorded. The difference of these image sets represents a background-corrected set, which is further processed by integrating each image along the waveguide axis over 100 pixels to improve dynamic range and signal to noise ratio. This is possible because the diffraction patterns are inherently shift-invariant along this axis.

In order to measure the input illumination angles, we do an additional recording of the objective pupil plane by switching a converging lens in the imaging system, between the tube lens and the camera. The position of this lens is adjusted in order to get a sharp image of the condenser diaphragm, which is optically conjugated to the pupil plane of the objective. A first image of the entire pupil is recorded by illuminating the condenser with a flash lamp, defining a sharp disc representing the Fourier domain with a maximum NA of 1.4. Then, we record the positions of the centroids of the spot distributions obtained with each tilted illumination. The relative positions of these centroids inside the pupil give a precise estimation of the illumination angles.

The focus point of the objective lens is set to about 10 µm above the waveguide (with reference to the geometry outlined in Fig. 1(b)), to a plane where light diffracted by the guide has developed sufficient intensity contrast in its interference fringes. We note that the exact knowledge of the focus position is not required for the reconstruction. Any mismatch between assumed and true axial positions will merely cause a corresponding axial translation of the RI profile. This phase imaging approach is for instance exploited in methods using transport-of-intensity equation (TIE) [18,20] and avoids the requirement of direct phase measurements (e.g. interferometry), which set higher demands on mechanical stability, light source or detection system. A drawback of imaging under defocused conditions is that the diffraction patterns exhibit large lateral shifts at high illumination angles, which requires to image a sufficiently large field of view.

Optics EXPRESS

2.3. Reconstruction of refractive index profiles

A detailed description of our algorithm is provided in Supplement 1. Basically, it simulates the recorded diffraction patterns by numerically propagating 1D plane waves at all tomographic angles through the waveguide sample, which is initially assumed to have an RI contrast of zero.

The squared differences between recorded and simulated irradiance profiles and their gradients with respect to the refractive indices of all pixels on the grid are calculated and used in a proximal accelerated gradient descent.

The scheme we are using here was originally proposed several years ago [21] for diffraction tomography and more recently for retrieving the 3D refractive index profiles of biological samples from intensity images [22]. Compared to reconstructions based on the first Born and Rytov approximations [23,24], it does not suffer as much from limitations regarding RI contrast and gradients. Importantly, the scheme allows for regularization, which we find to be essential for retrieving artifact free RI profiles. Further information about recent developments on diffraction tomography can for instance be found in Refs. [25,26].

Compared to previous implementations, our method goes one step further in estimating spherical phase aberrations in the objective pupil jointly with the cross section of the object. Specifically, the even coefficients of a radial phase polynomial in the pupil are retrieved up to the 16th order. Spherical aberrations are common in high aperture imaging systems and can for instance arise from a refractive index mismatch between sample and immersion oil. We find that aberrations can visibly distort the information contained in high-angle recordings, thus partly negating the achievable reconstruction benefit if they are not considered in the reconstruction.

Conceptually, our approach is related to blind deconvolution. Similar implementations have for instance been realized for phase diversity [27], optical coherence tomography [28] or Fourier ptychography [29].

2.4. Cross-validation with en-face images of waveguide cross-sections

To validate the tomographic results, a transverse slice of the waveguide substrate is cut off and polished to a thickness of about 130 to 150 µm. After polishing, the exact thickness is inferred using a microscope. A widefield image of the slice is recorded under straight coherent illumination (see Fig. 1(c)), with the objective manually focused onto its top surface. While such a slice is still too thick to enable a direct measurement of the RI distribution (for instance using interferometry), it is nevertheless possible to compare this experimental image with a simulated one, derived from the tomographically estimated RI profile. To simulate such a view, a plane wave is numerically propagated using a split-step Fourier Beam Propagation Method (BPM, see Supplement 1 for details) through the retrieved RI profile over a distance matching the glass slice.

In order to compare the experimental and computed camera images I_{exp} and I_{sim}, we subtract their background intensity levels and normalize the resulting differential intensities to 1 according to the l_2–norm ($\sqrt{\sum I^2} = 1$). Then, we correct for an eventual rotation between the two images by finding the rotation angle which maximizes the cross-correlation $I_{\mathrm{sim}} \star I_{\mathrm{exp}}$. As a result, the value

$$M = \left\| I_{\mathrm{sim}} \star I_{\mathrm{exp}} \right\|_{\infty} \tag{1}$$

serves as a scalar reconstruction quality metric, taking values between 0 and 1 due to the normalization.

3. Results

Figure 2 summarizes quantitative results from the tomographic imaging of a direct laser written waveguide. A writing speed of 2 mm/s and a laser power of 35 mW were employed for its manufacturing.

Optics EXPRESS

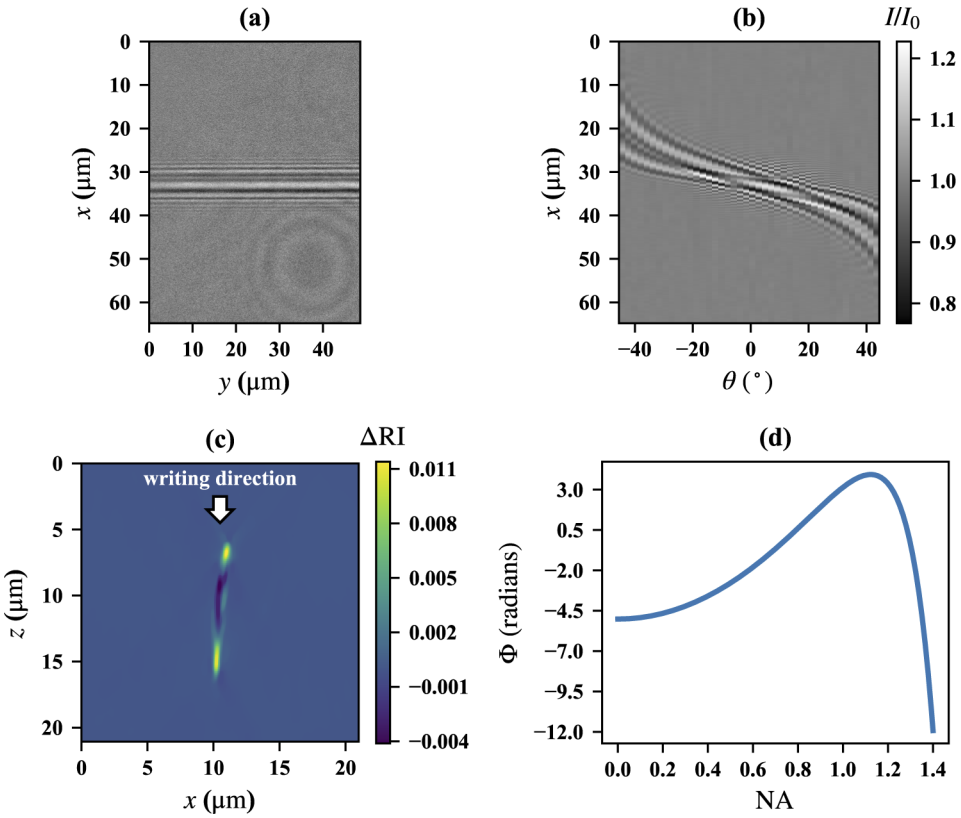

Fig. 2. Experimental results from tomographic waveguide imaging (a) defocused widefield view of the waveguide under straight coherent illumination ($\theta = 0$); (b) intensity tomogram used for the RI reconstruction; (c) reconstructed RI profile, showing regions of positive and negative contrast; (d) retrieved radial aberration phase in the pupil plane during the imaging; the RMS value over the entire 2D pupil is 3.5 rad.

Figure 2(a) shows a widefield view of the guiding structure under 10 μm defocus, (b) the intensity tomogram used for reconstruction. Each column of the tomogram is the sum of 100 columns in a widefield view taken at the illumination angle specified on the horizontal axis. (c) depicts the tomographic reconstruction of the RI profile, based on the tomogram shown in (b). The direction of laser writing is from the top. The RI variation ΔRI ranges from -0.004 to +0.011, clearly revealing spatially varying positive but also negative RI contrast. The coordinate $z = 0$ marks the sharply imaged focal plane for taking the raw images. Two main lobes of increased RI are visible, with a connecting narrow zone of negative RI contrast in between. Presumably, this split structure is caused by ion migration during the writing process [30]. The plot in Fig. 2(d) represents the jointly estimated radial aberration phase in the objective pupil during the tomographic imaging process. Defined over the full 2D pupil, it has an RMS value of 3.5 rad. This relatively high value is predominantly caused by the strong phase variation near the pupil edge. As we show later, this aberration leads to significant artifacts in the RI profile if it is neglected in the algorithmic reconstruction. Notably, for this particular case, we even find that a reconstruction based exclusively on low angle data (<30 deg.) shows a higher fidelity than the full angle data reconstruction without aberration estimation.

Experimental results from cross-validation of the reconstructed refractive index profile shown in Fig. 2(c) are summarized in Fig. 3. The figure contains an experimental widefield image of a

Optics EXPRESS

150 µm thick waveguide slice (a) together with its simulated counterpart (b). Both images are displayed in a logarithmic scale to highlight small differences. The images show a high similarity and also the reconstruction metric is correspondingly high with $M = 0.95$. Obviously, the narrow lobe-connecting zone of negative RI contrast is not noticeable in these images, presumably because the propagating light is mainly concentrated around the two lobes of increased RI, thus somewhat masking the zone in between them. To show that the RI of this connecting region has indeed been modified, we provide a different widefield view of the end facet (c), which has been constructed by adding multiple recordings taken under different illumination angles (rotated by ± 10 deg. around the x-axis and ±1 deg. around the z-axis with respect to the coordinate system shown in the image). Whilst only yielding qualitative information, this view reveals an RI modification of similar shape at the respective connecting zone (marked by an arrow), thus supporting the quantitative data shown in Fig. 2(c).

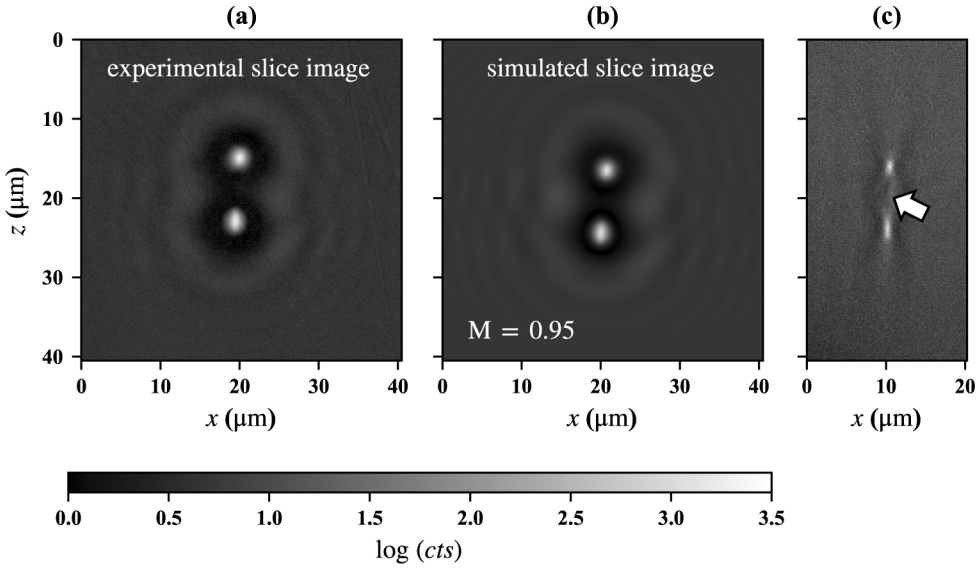

Fig. 3. Cross-validating the tomography results. (a) Experimental widefield image of a 150 µm thick waveguide slice; (b) Matching simulated view, based on the tomographic RI profile of Fig. 2(c). The image shows a high fidelity metric $M = 0.95$. Note that the images (a,b) are in log-scale. (c) The sum of many experimental widefield images from a range of illumination angles reveals a modified RI in the narrow zone between the main lobes (marked by arrow).

We have performed simulations on the sensitivity of M to errors in the RI profile in order to investigate the suitability of M as a fidelity metric. To this end, we deliberately altered the ΔRI profile of Fig. 2(c) by multiplying it with scaling factors between 0.5 and 1.5 and computed corresponding widefield slice images for comparison with the experimental image shown in Fig. 3(a). The M values for these simulated images are visualized by the blue curve in Fig. 4. The curve peaks at a scaling factor of 0.95, thus indicating that the profile of Fig. 2(c) could be slightly overestimated by 5%, i.e., absolute changes ΔRI in the reconstructed profile of only up to $5 \cdot 10^{-4}$. The curve further indicates that a potential over- or underestimation of the ΔRI change by about 20% would lead to a significant drop of M. The fact that we do not observe such a drop validates our tomographic approach and supports the suitability of M as a metric to quantitatively evaluate the tomographic reconstructions.

For further analysis, we have only incorporated images taken at small angles <30 deg. (NA = 0.5) for the tomographic reconstruction. This renders the inverse problem less well-posed,

Optics EXPRESS

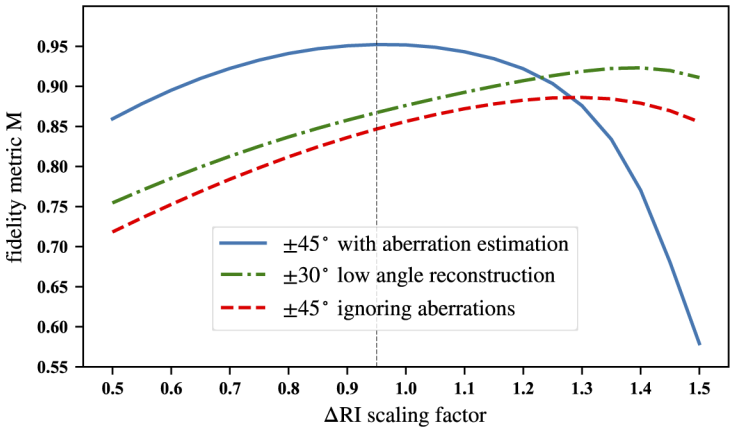

Fig. 4. Investigation on the suitability of *M* as fidelity metric. The blue curve at the top shows the influence of re-scaling the RI profile of Fig. 2(c) on *M*. The curve peaks around a scaling factor of 0.95, thus validating our tomographic approach. Similar curves are shown for tomographic reconstructions which have been intentionally degraded, either by incorporating only small angle recordings (green dash-dotted curve) or ignoring aberrations in the tomographic reconstruction (red dashed curve).

such that typical "hourglass" artifacts appear (see Fig. 5(a)). Another noticeable artifact is that the ΔRI change of the upper lobe appears to be about 30% smaller compared to the high-angle reconstruction of Fig. 2(c). If this reduced ΔRI value were real, it would cause this lobe to confine less light and consequently appear significantly dimmer in the slice image, which is proven by the simulation in Fig. 5(c). The *M* value of this simulated slice image and the experimental slice image of Fig. 3(a) is only 0.88, which indicates that the ΔRI value of the upper lobe must indeed be higher than predicted by the low-angle reconstruction. Re-scaling the ΔRI change as before (green dash-dotted line in Fig. 4) can only marginally increase the *M* value.

The low-angle simulations are interesting, because they show the reconstruction quality that can be expected if only dry optics (air objective and condenser) are used for the measurements. Objective lenses used for waveguide writing are often of this type and it would be attractive to characterize directly at the stage of fabrication, using the writing optics for tomography.

Finally, we investigate the importance of including phase aberrations in the tomographic reconstruction. For this reason, we again derived an RI profile from the intensity images in Fig. 2(b), but this time without jointly estimating aberrations. The result shown in Fig. 5(b) shows even more pronounced streak artifacts than the low-angle reconstruction. The impact on the simulated slice image (see Fig. 5(d)) is likewise more severe and reduces *M* to merely 0.85. Again, re-scaling ΔRI is unable to significantly increase *M* (red dashed line in Fig. 4).

We note that the retrieved aberration magnitude is negligibly small for the low-angle reconstruction, which in turn means that ignoring aberrations in this case has very little effect on the final RI profile. If aberrations are not incorporated in the high-angle reconstruction, however, the final result is of even lower quality than the low-angle reconstruction.

To further demonstrate the capabilities of our tomographic approach, we have applied it to a set of additional waveguides. All these additional structures were similarly fabricated at 150 µm depth in Corning Eagle glass, yet were manufactured using different settings for the laser power and write speed ("medium" = 35 mW and 2mm/s; "high" = 75 mW and 25 mm/s). Furthermore, for each power/speed setting different values of aberration phase were applied in the pupil plane of the laser fabrication objective lens. The laser writing system was initially optimised for phase aberrations using a sensorless scheme based on the material modification threshold [31],

Optics EXPRESS

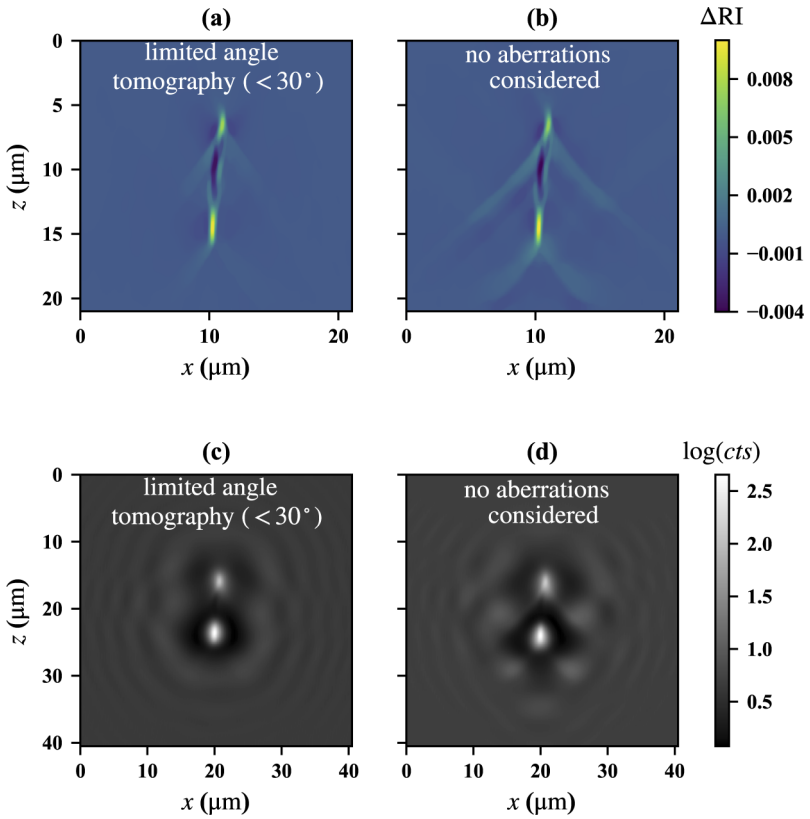

Fig. 5. Intentionally degraded tomographic reconstructions and their simulated slice images. The estimated phase profiles show typical "hourglass" artifacts due to incorporating only limited angles (a) or ignoring aberrations (b) in the reconstruction algorithm. Computed slice images based on these erroneous profiles (c, d) clearly differ from that of the best possible profile as well as the experimental image shown in Fig. 3.

representing the "min" data in the middle column of Fig. 6. The SLM was then also used to intentionally apply "negative" = -0.85 rad and "positive" = +0.85 rad of of primary spherical Zernike aberration. We emphasize that these aberration settings refer to the laser writing process and not to the tomographic characterization as discussed above.

Each of the six profiles in Fig. 6 corresponds to a unique combination of fabrication parameters, which obviously have a strong impact on shape and magnitude of the induced RI modifications. The tomography reveals fine spatial details at a resolution of a few hundred nm (e.g. a fine line of RI increase connecting the two main lobes in (f)) and RI variations below 10^{-3}. The highest RI change of +0.011 is obtained at "medium" laser power and lower speed with optimal spherical aberration compensation ("min"). It is also noticeable that both, a higher power setting and non-optimal aberration compensation, lead to an increased stretch of the RI modifications along the writing direction. Furthermore, there is clear difference between the measured waveguide cross-sections for positive and negative values of applied spherical aberration, in line with recent studies suggesting that minimal spherical aberration is not necessarily best for waveguide fabrication [32,33], and that this should be an additional parameter to tune during optimisation.

A comparison between the recorded and computed slice images for the waveguides shown in Fig. 6 are provided in Fig. 7. As before, the simulated and experimental slice images are

Optics EXPRESS

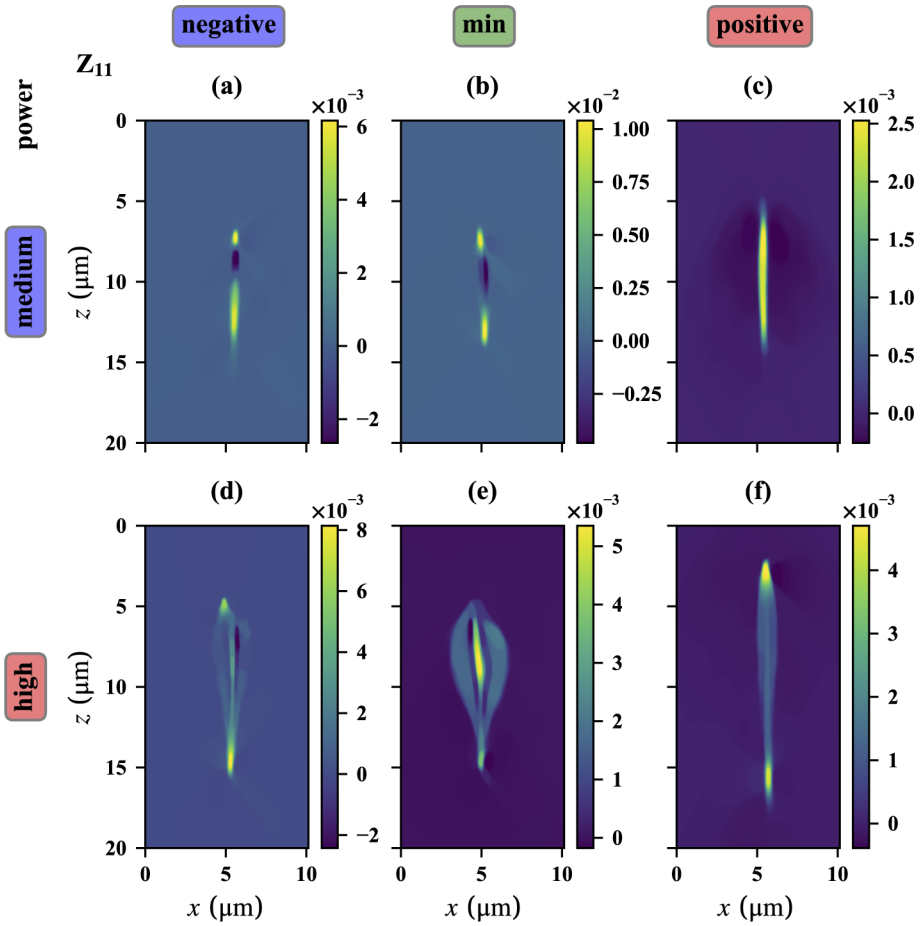

Fig. 6. RI profiles of waveguides manufactured at different fabrication settings. Each of the shown profiles corresponds to a unique combination of laser power ("medium" ≈ 35 mW, "high" ≈ 75 mW) and spherical aberration compensation ("min" = aberration minimal, "negative" = -0.85 rad, "positive" = +0.85 rad) during the writing process.

matching closely and the *M* values correspondingly high, showing general applicability of our tomographic technique for a wide variety of waveguide structures.

Optics EXPRESS

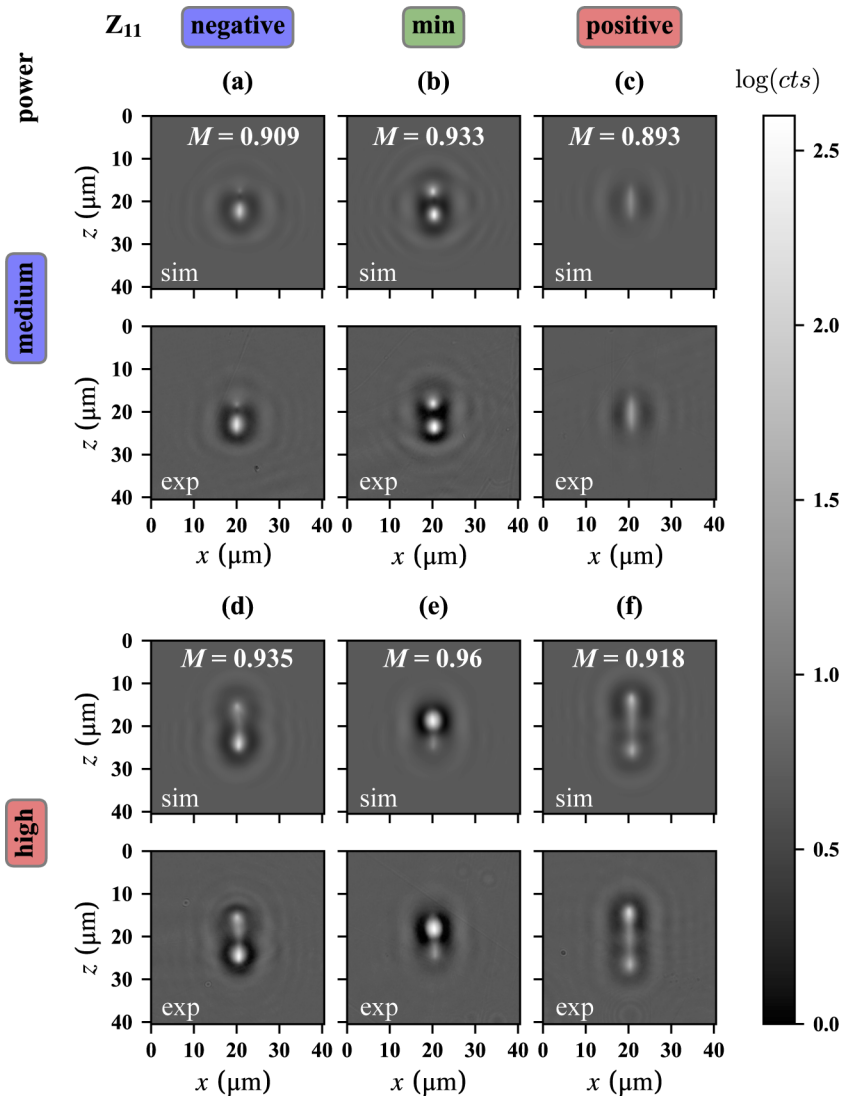

Fig. 7. Comparison of experimental and computed slice images of the waveguides in Fig. 6. The experimental images are below the respective simulations. The M values are shown as insets.

Optics EXPRESS

4. Summary and discussion

We have introduced a new tomographic approach for quantitative RI profilometry of laser written waveguides, which is able to retrieve spatial details on the order of a few hundred nanometers and an RI resolution of better than 10^{-3}. It can characterise waveguide profiles in a non-destructive manner at any point in a photonic circuit. We prove the validity of our technique by comparing en-face widefield images of thin waveguide slices with corresponding computed views based on the estimated RI profiles. Our technique is relatively simple to implement and requires only intensity images obtained from an LED illumination. It is further capable of jointly estimating pupil phase aberrations with the profiles. We have shown that it is important to take these aberrations into account in order to exploit the information collected at high tomographic angles.

We have further investigated the loss in quality of the reconstructed waveguide profiles caused by using only the low tomographic angles accessible by air optics and find that while the overall profile characteristics are preserved, the RI tends to be systematically underestimated. Nevertheless, it is likely that using more suitable regularization can improve on the accuracy in such scenarios. Then, it would be an attractive perspective to perform the tomographic quality assessment in situ, i.e., directly at the fabrication platform. For instance, the same objective lens could be used for writing and imaging photonic structures, and a dichroic mirror behind the objective could be used to separate writing and imaging paths. A practical challenge is the design of a suitable sample stage, which must permit the inclusion of a condenser lens at close proximity to the sample. Here, one could imagine to clamp the specimen from two sides, such that there is only air between its bottom surface and the condenser, or to place the sample on a sufficiently thin transparent holder.

In our current implementation, tomographic imaging and computational reconstruction speeds are insufficient to facilitate a real time quality control of laser written waveguides. A single tomographic reconstruction takes a few tens of seconds on the GPU. However, if trade-offs in reconstruction quality are tolerable, it is possible to drastically reduce the number of required views and also the time required for tomographic reconstructions. Should real-time characterization become feasible, it opens further interesting possibilities, such as a closed-loop control of laser parameters to ensure an optimal fabrication quality.

The investigations presented in this paper focus on the tomographic characterization of single waveguides without other photonic structures in close proximity. Preliminary tests on more complex structures such as small waveguide arrays using the same algorithm and similar regularization parameters showed the appearance of reconstruction artifacts. Likewise, we found the joint estimation of aberrations to be less reliable. A possible solution for the aberration estimation would be to fabricate an additional, isolated waveguide into the glass chip for which we can estimate the aberrations jointly, and then apply the retrieved aberration mask to the reconstruction of the waveguide array.

Funding. Engineering and Physical Sciences Research Council (EP/R004803/01); Deutsche Forschungsgemeinschaft (Schm2115/76-1); Austrian Science Fund (I3984-N36).

Disclosures. The authors declare no conflicts of interest.

Data availability. Data underlying the results presented in this paper are not publicly available at this time but may be obtained from the authors upon reasonable request.

Supplemental document. See Supplement 1 for supporting content.

References

1. R. Osellame, G. Cerullo, and R. Ramponi, *Femtosecond laser micromachining: photonic and microfluidic devices in transparent materials*, vol. 123 (Springer Science & Business Media, 2012).
2. Y. Shimotsuma, P. G. Kazansky, J. Qiu, and K. Hirao, "Self-organized nanogratings in glass irradiated by ultrashort light pulses," Phys. Rev. Lett. **91**(24), 247405 (2003).
3. S. Juodkazis, H. Misawa, T. Hashimoto, E. G. Gamaly, and B. Luther-Davies, "Laser-induced microexplosion confined in a bulk of silica: Formation of nanovoids," Appl. Phys. Lett. **88**(20), 201909 (2006).

Optics EXPRESS

4. T. Hashimoto, S. Juodkazis, and H. Misawa, "Void formation in glasses," New J. Phys. **9**(8), 253 (2007).
5. Y. Kondo, J. Qiu, T. Mitsuyu, K. Hirao, and T. Yoko, "Three-dimensional microdrilling of glass by multiphoton process and chemical etching," Jpn. J. Appl. Phys. **38**(Part 2, No. 10A), L1146–L1148 (1999).
6. C. Hnatovsky, R. Taylor, E. Simova, P. Rajeev, D. Rayner, V. Bhardwaj, and P. Corkum, "Fabrication of microchannels in glass using focused femtosecond laser radiation and selective chemical etching," Appl. Phys. A **84**(1-2), 47–61 (2006).
7. M. Shimizu, Y. Shimotsuma, M. Sakakura, T. Yuasa, H. Homma, Y. Minowa, K. Tanaka, K. Miura, and K. Hirao, "Periodic metallo-dielectric structure in diamond," Opt. Express **17**(1), 46–54 (2009).
8. S. Kang, K. Vora, and E. Mazur, "One-step direct-laser metal writing of sub-100 nm 3d silver nanostructures in a gelatin matrix," Nanotechnology **26**(12), 121001 (2015).
9. B. Dorin, P. Parkinson, and P. Scully, "Direct laser write process for 3d conductive carbon circuits in polyimide," J. Mater. Chem. C **5**(20), 4923–4930 (2017).
10. M. Saunders, "Optical fiber profiles using the refracted near-field technique: a comparison with other methods," Appl. Opt. **20**(9), 1645–1651 (1981).
11. M. Young, "Optical fiber index profiles by the refracted-ray method (refracted near-field scanning)," Appl. Opt. **20**(19), 3415–3422 (1981).
12. V. R. Bhardwaj, E. Simova, P. Corkum, D. Rayner, C. Hnatovsky, R. Taylor, B. Schreder, M. Kluge, and J. Zimmer, "Femtosecond laser-induced refractive index modification in multicomponent glasses," J. Appl. Phys. **97**(8), 083102 (2005).
13. Y. Youk and D. Y. Kim, "A simple reflection-type two-dimensional refractive index profile measurement technique for optical waveguides," Opt. Commun. **262**(2), 206–210 (2006).
14. E. Bélanger, J.-P. Bérubé, B. de Dorlodot, P. Marquet, and R. Vallée, "Comparative study of quantitative phase imaging techniques for refractometry of optical waveguides," Opt. Express **26**(13), 17498–17510 (2018).
15. W. Gorski and W. Osten, "Tomographic imaging of photonic crystal fibers," Opt. Lett. **32**(14), 1977–1979 (2007).
16. T. Kozacki, R. Krajewski, and M. Kujawińska, "Reconstruction of refractive-index distribution in off-axis digital holography optical diffraction tomographic system," Opt. Express **17**(16), 13758–13767 (2009).
17. A. C. Sullivan, "Tomographic characterization of volume photopolymers for integrated optics," Ph.D. thesis, University of Colorado at Boulder (2008).
18. A. Jesacher, P. Salter, and M. Booth, "Refractive index profiling of direct laser written waveguides: tomographic phase imaging," Opt. Mater. Express **3**(9), 1223–1232 (2013).
19. N. Bisch, J. Guan, M. J. Booth, and P. S. Salter, "Adaptive optics aberration correction for deep direct laser written waveguides in the heating regime," Appl. Phys. A **125**(5), 364 (2019).
20. M. R. Teague, "Deterministic phase retrieval: a green's function solution," J. Opt. Soc. Am. **73**(11), 1434–1441 (1983).
21. U. S. Kamilov, I. N. Papadopoulos, M. H. Shoreh, A. Goy, C. Vonesch, M. Unser, and D. Psaltis, "Optical tomographic image reconstruction based on beam propagation and sparse regularization," IEEE Trans. Comput. Imaging **2**(1), 59–70 (2016).
22. S. Chowdhury, M. Chen, R. Eckert, D. Ren, F. Wu, N. Repina, and L. Waller, "High-resolution 3d refractive index microscopy of multiple-scattering samples from intensity images," Optica **6**(9), 1211–1219 (2019).
23. E. Wolf, "Three-dimensional structure determination of semi-transparent objects from holographic data," Opt. Commun. **1**(4), 153–156 (1969).
24. P. Müller, M. Schürmann, and J. Guck, "The theory of diffraction tomography," arXiv preprint arXiv:1507.00466 (2015).
25. D. Jin, R. Zhou, Z. Yaqoob, and P. T. So, "Tomographic phase microscopy: principles and applications in bioimaging," J. Opt. Soc. Am. B **34**(5), B64–B77 (2017).
26. T.-A. Pham, E. Soubies, A. Goy, J. Lim, F. Soulez, D. Psaltis, and M. Unser, "Versatile reconstruction framework for diffraction tomography with intensity measurements and multiple scattering," Opt. Express **26**(3), 2749–2763 (2018).
27. R. G. Paxman, T. J. Schulz, and J. R. Fienup, "Joint estimation of object and aberrations by using phase diversity," J. Opt. Soc. Am. A **9**(7), 1072–1085 (1992).
28. A. Kumar, W. Drexler, and R. A. Leitgeb, "Subaperture correlation based digital adaptive optics for full field optical coherence tomography," Opt. Express **21**(9), 10850–10866 (2013).
29. J. Chung, J. Kim, X. Ou, R. Horstmeyer, and C. Yang, "Wide field-of-view fluorescence image deconvolution with aberration-estimation from fourier ptychography," Biomed. Opt. Express **7**(2), 352–368 (2016).
30. T. Fernandez, M. Sakakura, S. Eaton, B. Sotillo, J. Siegel, J. Solis, Y. Shimotsuma, and K. Miura, "Bespoke photonic devices using ultrafast laser driven ion migration in glasses," Prog. Mater. Sci. **94**, 68–113 (2018).
31. R. D. Simmonds, P. S. Salter, A. Jesacher, and M. J. Booth, "Three dimensional laser microfabrication in diamond using a dual adaptive optics system," Opt. Express **19**(24), 24122–24128 (2011).
32. T. T. Fernandez, J. Siegel, J. Hoyo, B. Sotillo, P. Fernandez, and J. Solis, "Controlling plasma distributions as driving forces for ion migration during fs laser writing," J. Phys. D: Appl. Phys. **48**(15), 155101 (2015).
33. P. Ferreira, G. Almeida, and C. Mendonça, "A simple strategy for increasing optical waveguide performance using spherical aberration," Opt. & Laser Technol. **142**, 107235 (2021).